marine drugs

MDPI

Article

Marinoacrebols A–D, New Peptaibol-like Peptides Isolated from a Marine-Derived Fungus, *Acremonium persicinum* ACE-015

Davin Cha [1,†], Anika Nishat Mohona [2,3,†], Eun-Young Lee [4], Yun Seo Park [5], Ji Young Lee [6], Han-Seul Chang [1], Si-Yeon Kim [1], Myung-Ji Jung [1], Hanna Kim [1], Joo-Won Nam [2], Grace Choi [7], Se-Young Son [4], Sun-Shin Cha [1,4], Sang Hee Shim [5], Songyi Lee [8,9], Hyukjae Choi [2,3,*] and Sang-Jip Nam [1,4,*]

1 Graduate Program in Innovative Biomaterials Convergence, Ewha Womans University, Seoul 03760, Republic of Korea; dvdv827@naver.com (D.C.); onethree0510@naver.com (H.-S.C.); siyeon9021@gmail.com (S.-Y.K.); ji5418@naver.com (M.-J.J.); khanna9248@gmail.com (H.K.); chajung@ewha.ac.kr (S.-S.C.)
2 College of Pharmacy, Yeungnam University, Gyeongsangbukdo 38541, Republic of Korea; nishatmohona554@gmail.com (A.N.M.); jwnam@yu.ac.kr (J.-W.N.)
3 Research Institute of Cell Culture, Yeungnam University, Gyeongsangbukdo 38541, Republic of Korea
4 Department of Chemistry and Nanoscience, Ewha Womans University, Seoul 03760, Republic of Korea; younglee0124@naver.com (E.-Y.L.); thstpdud1@naver.com (S.-Y.S.)
5 Natural Products Research Institute, College of Pharmacy, Seoul National University, Seoul 08826, Republic of Korea; asdddbs@snu.ac.kr (Y.S.P.); sanghee_shim@snu.ac.kr (S.H.S.)
6 Institute of Sustainable Earth and Environmental Dynamics (SEED), Pukyong National University, Busan 48547, Republic of Korea; jji123789@naver.com
7 Department of Marine Ecological Biotechnology, Kunsan National University, Gunsan 54150, Republic of Korea; gchoi@kunsan.ac.kr
8 Department of Chemistry, Pukyong National University, Busan 48513, Republic of Korea; slee@pknu.ac.kr
9 Industry 4.0 Convergence Bionics Engineering, Pukyong National University, Busan 48513, Republic of Korea
* Correspondence: h5choi@yu.ac.kr (H.C.); sjnam@ewha.ac.kr (S.-J.N.); Tel.: +82-53-810-2824 (H.C.); +82-2-3277-6805 (S.-J.N.)
† These authors contributed equally to this work.

Abstract

Four new peptaibol-like peptides, marinoacrebols A–D (**1**–**4**), were isolated from the marine-derived fungus *Acremonium persicinum* ACE-015. Their planar structures were elucidated through comprehensive spectroscopic analyses, including 1D and 2D nuclear magnetic resonance (NMR) experiments, together with high-resolution mass spectrometry. Detailed analysis of COSY and HMBC correlations, supported by electrospray ionization tandem mass spectrometry (ESI-MS/MS) fragmentation data, enabled the determination of their amino acid sequences. Marinoacrebols A–C (**1**–**3**) were identified as 19-residue peptides, whereas marinoacrebol D (**4**) was identified as an 18-residue peptide. The absolute configurations of the chiral amino acid residues were determined using advanced Marfey's analysis, while electronic circular dichroism (ECD) analysis supported a right-handed helical conformation. Compounds **1**–**4** exhibited selective antibacterial activity against Gram-positive bacteria, with minimum inhibitory concentration (MIC) values ranging from 8–64 μg/mL. Notably, compound **2** showed the strongest antibacterial activity against *Kocuria rhizophila* KCTC 1915, with an MIC value of 8 μg/mL.

Keywords: *Acremonium persicinum*; peptides; Marfey's method

Check for updates

Academic Editor: Simona De Marino

Received: 18 September 2026
Revised: 5 November 2026
Accepted: 7 November 2026
Published: 10 November 2026

Copyright: © 2026 by the authors. Licensee MDPI, Basel, Switzerland. This article is an open access article distributed under the terms and conditions of the Creative Commons Attribution (CC BY) license.

1. Introduction

Marine-derived fungi inhabit diverse ecological niches and represent a rich source of structurally unique secondary metabolites [1–3]. Adaptation to extreme and competitive

marine environments has enabled these organisms to produce a wide range of bioactive compounds with diverse chemical scaffolds and biological activities [4]. Among marine fungi, the genus *Acremonium* (family Hypocreaceae) has been reported from various habitats, including marine sediments, sponges, corals, and terrestrial environments [5–8]. Previous chemical investigations of *Acremonium* species have led to the discovery of structurally diverse secondary metabolites, including acremines, acremonidins, and acremolactones, encompassing terpenoids, polyketides, peptides, steroids, and alkaloids [6,9–11]. Notably, fungal peptide-based natural products often exhibit lower toxicity and fewer adverse effects than synthetic compounds, highlighting their potential as promising candidates for drug development [12].

Peptaibols are a distinctive class of nonribosomal peptides characterized by the presence of nonproteinogenic amino acids, such as α-aminoisobutyric acid (Aib) and isovaline (Iva) [13]. These residues play important roles in stabilizing helical conformations and contribute to diverse biological activities, including antimicrobial and membrane-permeabilizing effects associated with transmembrane pore formation [14,15]. Unlike ribosomally synthesized and post-translationally modified peptides (RiPPs), nonribosomal peptides (NRPs) are assembled by nonribosomal peptide synthetases (NRPSs), which enable the incorporation of a broad range of nonproteinogenic amino acids and thereby greatly expand their structural diversity [13,16]. Although cyclic peptides are predominant among marine fungal metabolites, linear peptides such as peptaibols remain relatively rare, making their discovery valuable for expanding the chemical diversity of marine natural products [17]. In particular, the structural diversity and biological relevance of these peptides have attracted considerable attention in recent years because of their potential pharmaceutical applications [14].

As part of our ongoing investigation of bioactive secondary metabolites from marine-derived fungi, chemical investigation of the marine-derived fungus *Acremonium persicinum* strain ACE-015 yielded four new peptaibol-like peptides, marinoacrebols A–D (**1**–**4**, Figure 1). Here, we report their isolation, detailed structural elucidation based on spectroscopic analyses, and evaluation of their antibacterial activities.

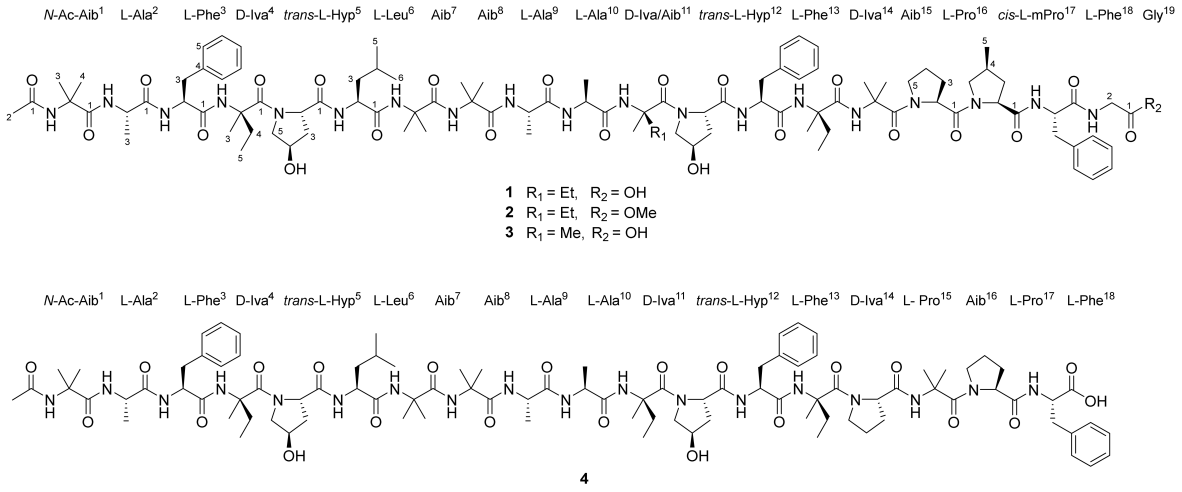

Figure 1. Structures of compounds **1**–**4**. Superscript numbers indicate the positions of the amino acid residues in the peptide sequences.

2. Results and Discussion

2.1. Structure Elucidation

Marinoacrebol A (**1**) was isolated as a white amorphous powder, and its molecular formula was determined to be $C_{98}H_{145}N_{19}O_{23}$ based on HR-ESI-MS data, which showed a

$[M - H]^-$ ion at m/z 1955.0595 (calcd for $C_{98}H_{144}N_{19}O_{23}^-$, 1955.0688). The molecular formula corresponds to 36 degrees of unsaturation, consistent with a highly functionalized peptide structure. The ^1H nuclear magnetic resonance (NMR) spectrum displayed characteristic signals for peptide-derived protons, including 15 amide NH protons (δ_H 7.56–8.49) and 13 α-proton signals (δ_H 3.93–4.68). Although amide protons generally undergo H/D exchange in MeOD and are therefore often not observed, some amide proton resonances can remain detectable due to slower exchange associated with intramolecular hydrogen bonding and conformational restriction within the peptide structure [18]. The same observation was observed for compounds **2**–**4**, with amide NH proton signals remaining detectable in MeOD under similar conditions. Multiple methyl signals and aliphatic methine and methylene resonances further supported the presence of a peptide framework containing both proteinogenic and nonproteinogenic amino acids. The ^{13}C NMR, DEPT, and HSQC spectra revealed 98 carbon signals, including 20 carbonyl carbons (δ_C 172.2–178.7), indicating a 19-residue peptide backbone (Table 1).

Table 1. NMR Data for Marinoacrebol A (**1**) in MeOD.

Unit	Position	Marinoacrebol A (1) [a]			
		δ_C, Type	**δ_H, Mult [b] (*J* in Hz)**	**COSY**	**HMBC**
Ac	1	173.4, C			
	2	23.4, CH_3	2.10, s		Ac-1
Aib^1	NH		8.49, s		Ac-1, Aib^1-1, Aib^1-2
	1	178.6, C			
	2	57.4, C			
	3	26.1, CH_3	1.51 *, m		Aib^1-1, Aib^1-2
	4	26.8, CH_3	1.49, s		Aib^1-1, Aib^1-2
Ala^2	NH		8.34, d (3.9)	Ala^2-2	Aib^1-1
	1	176.1, C			
	2	52.9, CH	3.97 *, m	Ala^2-NH	Ala^2-1
	3	16.7, CH_3	1.14, d (7.4)		Ala^2-1, Ala^2-2
Phe^3	NH		8.22, d (8.5)	Phe^3-2	Ala^2-1
	1	174.1, C			
	2	56.9, CH	4.52 *, m	Phe^3-NH, Phe^3-3	
	3	38.1, CH_2	3.33 *, m; 3.13, dd (14.2, 11.9)	Phe^3-2	Phe^3-1, Phe^3-4, Phe^3-5
	4	139.0, C			
	5/5′	129.9, CH	7.24 *, m		Phe^3-7
	6/6′	129.5, CH	7.24 *, m		Phe^3-4
	7	127.9, CH	7.20 *, m		
Iva^4	NH		7.79, s		Phe^3-1, Iva^4-2, Iva^4-5
	1	176.2, C			
	2	60.6, C			
	3	29.9, CH_2	2.30, q (7.4); 1.93 *, m	Iva^4-4	Iva^4-1, Iva^4-2
	4	8.0, CH_3	0.94 *, m	Iva^4-3	
	5	20.5, CH_3	1.59 *, m		Iva^4-2
Hyp^5	OH	not obsd			
	1	176.2, C			
	2	63.3, CH	4.57, t (9.5)	Hyp^5-3	Hyp^5-1
	3	38.0, CH_2	2.35 *, m; 1.83 *, m	Hyp^5-2, Hyp^5-4	
	4	71.3, CH	4.45 *, m	Hyp^5-3, Hyp^5-5	Hyp^5-5
	5	58.4, CH_2	3.88 *, m; 3.57 *, m	Hyp^5-4	Hyp^5-2

Table 1. *Cont.*

Unit	Position	Marinoacrebol A (1) [a]			
		δ_C, Type	δ_H, Mult [b] (*J* in Hz)	COSY	HMBC
Leu^6	NH		7.97, d (6.7)		Hyp^5-1, Leu^6-2
	1	175.9, C			
	2	55.7, CH	4.10 *, m	Leu^6-3	Leu^6-1
	3	40.4, CH_2	1.93 *, m	Leu^6-2	Leu^6-5, Leu^6-6
			1.63 *, m		
	4	26.2, CH	1.83 *, m	Leu^6-5, Leu^6-6	Leu^6-3
	5	23.8, CH_3	1.06, d (6.7)	Leu^6-4	
	6	21.5, CH_3	0.94 *, m	Leu^6-4	
Aib^7	NH		7.62, s		Leu^6-1, Aib^7-2, Aib^7-3
	1	177.6, C			
	2	57.8, C			
	3	23.9, CH_3	1.49 *, m		Aib^7-1, Aib^7-2
	4	26.9, CH_3	1.57, s		Aib^7-1, Aib^7-2
Aib^8	NH		7.74, s		Aib^7-1, Aib^8-1, Aib^8-2
	1	178.6, C			
	2	57.8, C			
	3	23.4, CH_3	1.52 *, m		Aib^8-1, Aib^8-2
	4	27.6, CH_3	1.55 *, m		Aib^8-1, Aib^8-2
Ala^9	NH		7.88, d (5.8)		Aib^8-1, Ala^9-2, Ala^9-3
	1	176.4, C			
	2	53.0, CH	4.16 *, m	Ala^9-3	Ala^9-1
	3	16.9, CH_3	1.59 *, m	Ala^9-2	Ala^9-1
Ala^{10}	NH		8.06, d (7.4)	Ala^{10}-2	Ala^9-1, Ala^{10}-2
	1	175.7, C			
	2	51.4, CH	4.52 *, m	Ala^{10}-NH, Ala^{10}-3	Ala^9-1, Ala^{10}-1
	3	17.7, CH_3	1.55 *, m	Ala^{10}-2	Ala^{10}-2
Iva^{11}	NH		7.80, s		Ala^{10}-1, Iva^{11}-1, Iva^{11}-2
	1	174.3, C			
	2	61.9, C			
	3	30.5, CH_2	2.24, q (7.4);	Iva^{11}-4	Iva^{11}-1, Iva^{11}-2
			1.93 *, m		
	4	8.6, CH_3	0.90 *, m	Iva^{11}-3	
	5	24.5, CH_3	1.51 *, m		Iva^{11}-2
Hyp^{12}	OH	not obsd			
	1	174.7, C			
	2	62.7, CH	4.40, t (8.7)	Hyp^{12}-3	Hyp^{12}-1
	3	37.7, CH_2	2.03 *, m;	Hyp^{12}-2, Hyp^{12}-4	
			0.97 *, m		
	4	70.8, CH	4.21 *, m	Hyp^{12}-3, Hyp^{12}-5	
	5	58.1, CH_2	3.87 *, m	Hyp^{12}-4	Hyp^{12}-2
			3.48, dd (12.5, 1.6);		
Phe^{13}	NH		8.12 *, m	Phe^{13}-2	Hyp^{12}-1
	1	175.6, C			
	2	56.0, CH	4.52 *, m	Phe^{13}-NH, Phe^{13}-3	Phe^{13}-1
	3	37.7, CH_2	3.40, dd (14.3, 4.0);	Phe^{13}-2	Phe^{13}-2, Phe^{13}-4, Phe^{13}-5
			3.04, t (13.0)		
	4	139.6, C			
	5/5′	130.5, CH	7.35 *, m		Phe^{13}-7
	6/6′	129.6, CH	7.35 *, m		Phe^{13}-4
	7	127.6, CH	7.20 *, m		

Table 1. *Cont.*

Unit	Position	Marinoacrebol A (1) [a]			
		δ_C, Type	δ_H, Mult [b] (*J* in Hz)	COSY	HMBC
Iva^{14}	NH		7.56, s		Iva^{14}-1, Iva^{14}-2
	1	174.6, C			
	2	60.8, C			
	3	29.8, CH_2	2.32 *, m 1.93 *, m	Iva^{14}-4	Iva^{14}-2
	4	8.0, CH_3	0.94 *, m	Iva^{14}-3	
	5	20.9, CH_3	1.53 *, m		Iva^{14}-1, Iva^{14}-2
Aib^{15}	NH		8.12 *, m		
	1	178.7, C			
	2	57.5, C			
	3	23.9, CH_3	1.51 *, m		Aib^{15}-1, Aib^{15}-2
	4	26.9, CH_3	1.43, s		Aib^{15}-1, Aib^{15}-2
Pro^{16}	1	175.2, C			
	2	63.9, CH	4.68, t (7.6)		Pro^{16}-1, Pro^{16}-3, Pro^{16}-4
	3	30.3, CH_2	2.35 *, m; 1.83 *, m		Pro^{16}-1, Pro^{16}-5
	4	26.9, CH_2	1.99 *, m; 1.93 *, m		
	5	50.2 CH_2	3.87 *, m; 3.53 *, m		
mPro^{17}	1	174.5, C			
	2	64.8, CH	4.23, dd (10.7, 7.2)		mPro^{17}-1
	3	38.0, CH_2	2.14 *, m; 0.54, d (11.0)	mPro^{17}-4	mPro^{17}-2
	4	35.3, CH	2.14 *, m	mPro^{17}-3, mPro^{17}-5	
	5	16.6, CH_3	1.01, d (6.1)	mPro^{17}-4	mPro^{17}-3, mPro^{17}-4, mPro^{17}-5
	6	57.0, CH_2	3.97 *, m		
Phe^{18}	NH		8.12 *, m	Phe^{18}-2	mPro^{17}-1
	1	174.4, C			
	2	56.8, CH	4.46 *, m	Phe^{18}-NH, Phe^{18}-3	
	3	38.4, CH_2	3.30 *, m; 2.96, t (12.8)	Phe^{18}-2	Phe^{18}-4, Phe^{18}-5
	4	139.2, C			
	5/5′	130.3, CH	7.27, d (7.3)		Phe^{18}-7
	6/6′	129.7, CH	7.35 *, m		Phe^{18}-4
	7	128.7, CH	7.24 *, m		
Gly^{19}	NH		7.91, t (5.9)	Gly^{19}-2	
	1	172.2, C			
	2	42.0, CH_2	3.97 *, m; 3.93, dd (17.9, 5.5)	Gly^{19}-NH	Phe^{18}-1, Gly^{19}-1

[a] 900 MHz for ^{1}H NMR and 225 MHz for ^{13}C NMR. [b] Numbers of attached protons were determined by analysis of 2D spectra. * Overlapped signals.

Detailed analysis of the 2D NMR data enabled the identification of individual amino acid residues. The COSY spectrum revealed characteristic spin systems corresponding to alanine, phenylalanine, leucine, proline, and glycine residues. In addition, the presence of nonproteinogenic residues was established based on diagnostic NMR features. Aib residues were identified by their quaternary α-carbons and two methyl singlets, whereas Iva residues were assigned based on characteristic methyl and methylene correlations. Two

4-hydroxyproline (Hyp) residues were identified by their distinctive downfield-shifted methine carbon resonances and corresponding COSY correlations.

The sequence of amino acid residues was established through a combination of HMBC correlations and ESI-MS/MS fragmentation analysis. Key long-range HMBC correlations from amide NH protons to adjacent carbonyl carbons enabled the stepwise assignment of amino acid connectivity. HMBC correlations from the NH (δ_H 8.49, s) of Aib^1 to the acetyl carbonyl carbon, C-1 of Ac, and the quaternary carbon C-2 (δ_C 57.4) of Aib^1 established the linkage between Ac and Aib^1. The Ala^2 residue was assigned based on a COSY correlation between H-2 (δ_H 3.97, m) and NH (δ_H 8.34, d, J = 3.9 Hz) of Ala^2. This assignment was further supported by HMBC correlations from H-2 to C-1 (δ_C 176.1) and from H-3 (δ_H 1.14, d, J = 7.4 Hz) to C-2 (δ_C 52.9) and C-1. An HMBC correlation from the NH of Ala^2 to C-1 of Aib^1 established the connectivity between Aib^1 and Ala^2. The Phe^3 residue was identified through analysis of the COSY and HMBC NMR data. A COSY correlation was observed between the methine proton H-2 (δ_H 4.52, m) and the methylene protons H-3 (δ_H 3.13, dd, J = 2.41, 14.2 Hz; δ_H 3.33, m). HMBC correlations from H-3 to the unprotonated carbon C-4 (δ_C 139.0) and C-5/5′ (δ_C 129.9) were observed. The aromatic protons H-5/H-5′ (δ_H 7.23, m) and H-6/H-6′ (δ_H 7.24, m) also showed HMBC correlations with C-4. The ^{1}H and ^{13}C NMR chemical shifts of H-4 (δ_H 0.94, m; δ_C 8.0) indicated the presence of Iva^4. This assignment was supported by a COSY correlation between H-4 and H-3 (δ_H 2.30, m; δ_H 1.92, m), as well as HMBC correlations from H-5 (δ_H 1.59, m) and H-3 to C-2 (δ_C 60.6). HMBC correlations from the NH (δ_H 7.79, s) of Iva^4 to C-2 of Iva^4 and C-1 (δ_C 174.1) of Phe^3 established the linkage between Phe^3 and Iva^4. COSY correlations [H-2 (δ_H 4.57, t, J = 10.1, 9.0 Hz)/H-3 (δ_H 1.83, m; δ_H 2.35, m)/H-4 (δ_H 4.45, m)/H-5 (δ_H 3.57, m; δ_H 3.88, m)] revealed a contiguous spin system extending from H-2 to H-5 in Hyp^5. Comprehensive analysis of the 1D and 2D NMR data, particularly the methylene carbon resonances [C-3 (δ_C 38.0) and C-5 (δ_C 58.4)], indicated a proline-type scaffold. The attachment of a hydroxyl group at C-4 was supported by the significantly deshielded H-4 (δ_H 4.45, m) and C-4 (δ_C 71.3) resonances, allowing for the assignment of this residue as 4-hydroxyproline (Hyp^5). The Leu^6 residue was assigned based on COSY cross-peaks between the methyl group H-5 (δ_H 1.06, d, J = 6.7 Hz) and H-6 (δ_H 0.94, m) with H-4 (δ_H 1.82, m), as well as between H-2 (δ_H 4.10, m) and H-3 (δ_H 1.63, m; δ_H 1.93, m). This assignment was corroborated by HMBC correlations from H-4 to C-3 (δ_C 40.4) and from H-3 to C-5 (δ_C 23.8) and C-6 (δ_C 21.5). This residue was linked to Hyp^5 through an HMBC correlation from the NH (δ_H 7.97, d, J = 6.7 Hz) of Leu^6 to C-1 (δ_C 176.2) of Hyp^5. The Aib^7 and Aib^8 residues were identified by HMBC correlations from their *gem*-dimethyl groups [Aib^7: H-3 (δ_H 1.49, m), H-4 (δ_H 1.57, m); Aib^8: H-3 (δ_H 1.52, m), H-4 (δ_H 1.55, m)] to the responsible quaternary carbons (C-2) and carbonyl carbons (C-1). The linkages for Leu^6–Aib^7 and Aib^7–Aib^8 were confirmed by HMBC correlations from the NH protons of Aib^7 (δ_H 7.62, s) and Aib^8 (δ_H 7.74, s) to the carbonyl carbons of the preceding residues [Leu^6 C-1 (δ_C 175.9) and Aib^7 C-1 (δ_C 177.6), respectively]. The sequential Ala^9 and Ala^{10} residues were assigned based on COSY cross-peaks between H-2 and H-3 [Ala^9: δ_H 4.16/1.59; Ala^{10}: δ_H 4.52/1.55], supported by HMBC correlations from H-2 to C-1. The Aib^8–Ala^9 and Ala^9–Ala^{10} connectivities were established by HMBC correlations from the NH (δ_H 7.88) of Ala^9 to C-1 (δ_C 178.6) of Aib^8 and from the NH (δ_H 8.06) of Ala^{10} to C-1 (δ_C 176.4) of Ala^9. The presence of Iva^{11}, Iva^{14}, and a residue similar to Iva^4 was indicated by characteristic chemical shifts [C-4 (δ_C 8.0–8.6) and H-4 (δ_H 0.90–0.94)]. For Iva^{11}, the spin system was supported by COSY correlations between H-4 and H-3 (δ_H 1.94, 2.24) and HMBC correlations from H-5 (δ_H 1.51) and H-3 to C-2 (δ_C 61.9). The Ala^{10}–Iva^{11} linkage was established by an HMBC correlation from the NH (δ_H 7.80) of Iva^{11} to C-1 (δ_C 175.7) of Ala^{10}. The Hyp^{12} residue was identified by a contiguous COSY spin system extending from H-2 (δ_H 4.40) to H-5 (δ_H 3.48, 3.87), with the hydroxylation at C-4 evidenced by the

deshielded resonance at δ_C 71.3. The Phe[13] and Phe[18] residues were assigned based on COSY correlations between H-2 and H-3 and between H-2 and NH, together with HMBC correlations from the methylene protons (H-3) to the unprotonated aromatic carbons C-4 (δ_C 139.6/139.2). Their linkages were established by HMBC correlations from the NH of Phe[13] to C-1 of Hyp[12] and from the NH of Phe[18] to C-1 of mPro[17]. The Pro[16] and mPro[17] (4-methylproline) residues were characterized based on their respective COSY and HMBC correlations. For mPro[17], the 4-methyl group was confirmed by HMBC correlations from H-5 (δ_H 1.01) to C-3 (δ_C 38.0) and C-6 (δ_C 57.0). Finally, the C-terminal Gly[19] residue was identified by COSY correlations between the methylene protons H-2 (δ_H 3.97, 3.93) and NH (δ_H 7.91). The Phe[18]–Gly[19] linkage was established by an HMBC correlation from H-2 of Gly[19] to C-1 (δ_C 174.4) of Phe[18] (Figures S1–S7).

Further support for the sequence was obtained from ESI-MS/MS fragmentation data, which showed a series of b_n and y_n ions consistent with the proposed amino acid sequence. The observed fragmentation pattern was in good agreement with the assigned sequence, providing further evidence for the connectivity of the individual residues. Based on the combined spectroscopic evidence, the complete planar structure of marinoacrebol A (**1**) was established as *N*-Ac-Aib[1]-Ala[2]-Phe[3]-Iva[4]-Hyp[5]-Leu[6]-Aib[7]-Aib[8]-Ala[9]-Ala[10]-Iva[11]-Hyp[12]-Phe[13]-Iva[14]-Aib[15]-Pro[16]-mPro[17]-Phe[18]-Gly[19] (Figures 2A and 3A).

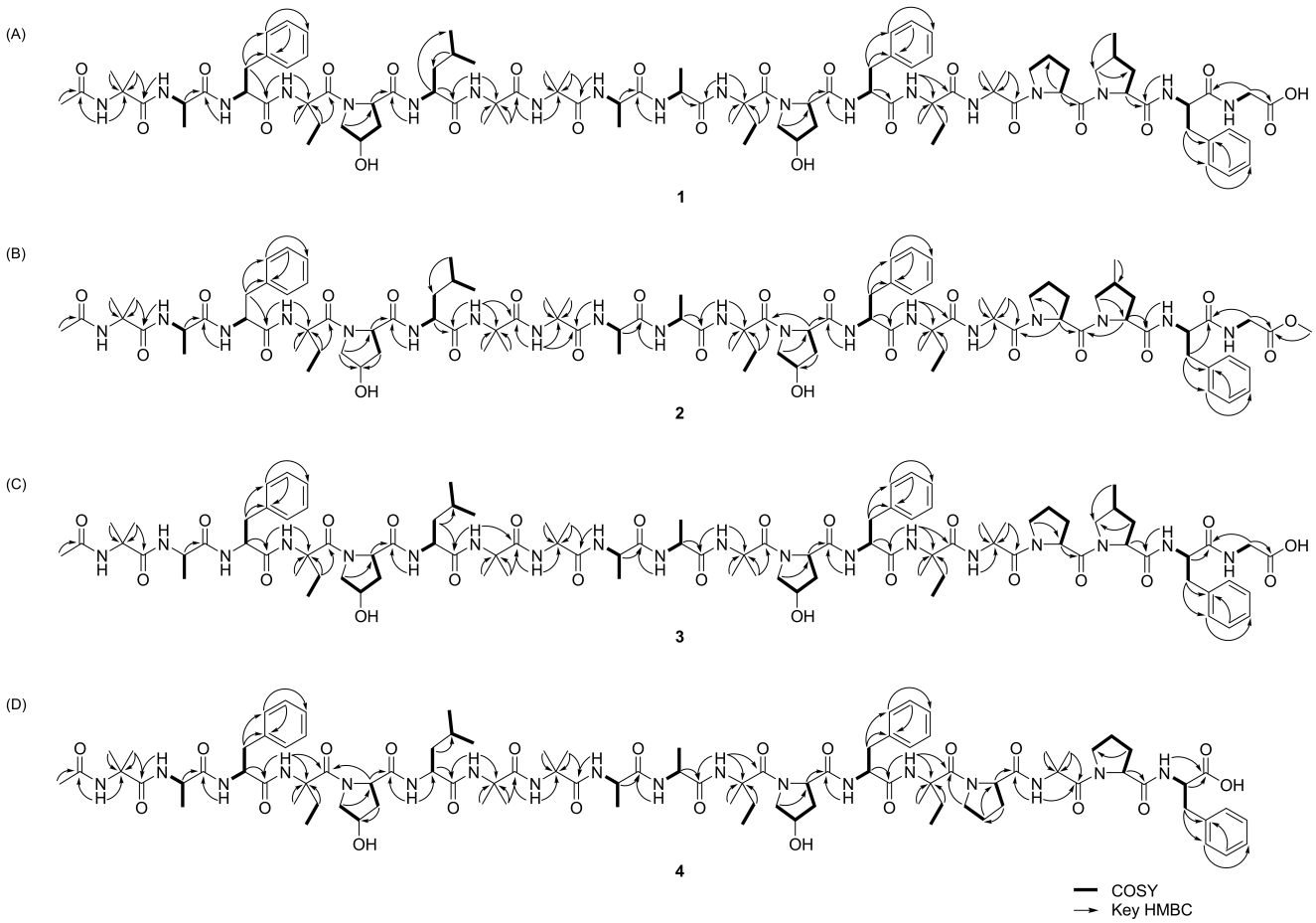

Figure 2. COSY and key HMBC correlations of **1**–**4**. (**A**) Marinoacrebol A (**1**); (**B**) Marinoacrebol B (**2**); (**C**) Marinoacrebol C (**3**); (**D**) Marinoacrebol D (**4**).

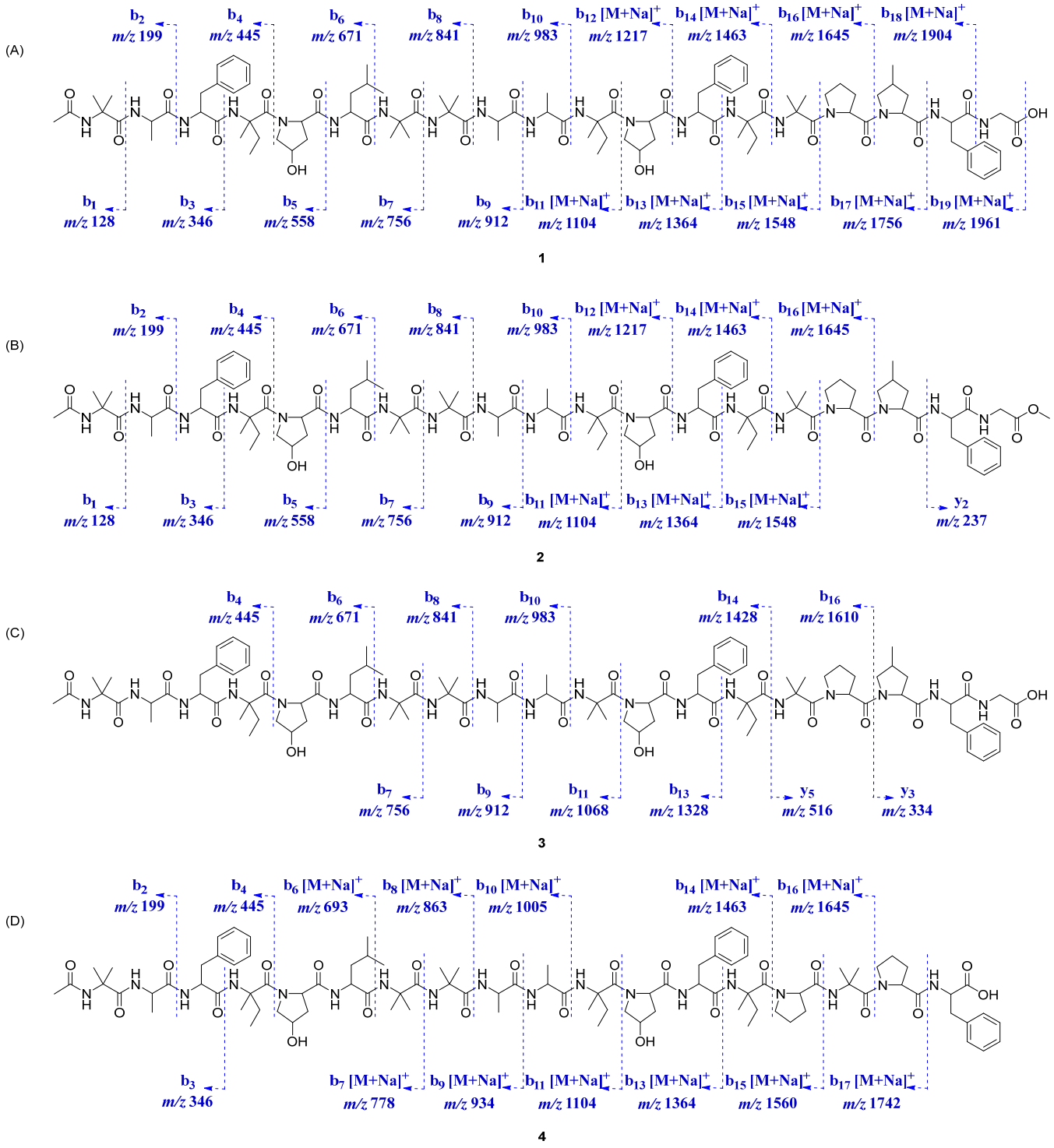

Figure 3. ESI-MS/MS fragmentation of **1**–**4**. (**A**) Marinoacrebol A (**1**); (**B**) Marinoacrebol B (**2**); (**C**) Marinoacrebol C (**3**); (**D**) Marinoacrebol D (**4**). Blue dashed indicated the peptide bond cleavage sites corresponding to the observed b_n- and y_n-type fragment ions.

Marinoacrebol B (**2**) was isolated as a white amorphous powder. Its molecular formula was established as $C_{99}H_{147}N_{19}O_{23}$ by HR-ESI-MS analysis, which showed a deprotonated molecular ion at m/z 1969.0777 $[M - H]^-$ (calcd for $C_{99}H_{146}N_{19}O_{23}^-$, 1969.0844), indicating that **2** contains one additional carbon and two additional hydrogen atoms relative to **1**. This difference suggested a minor structural modification without alteration of the overall peptide framework. The ^{1}H NMR spectrum of **2** exhibited 15 exchangeable NH protons (δ_H 7.56–8.49) along with 13 α-proton signals (δ_H 3.99–4.69), while the ^{13}C NMR and HSQC

spectra revealed 99 carbon resonances, including 20 carbonyl carbons (δ_C 171.1–178.7), consistent with a 19-residue peptide closely related to marinoacrebol A (**1**) (Figures S10–S15).

Comparison of the NMR data of **2** with those of **1** showed that the resonances attributable to the peptide backbone were essentially superimposable, indicating that the amino acid sequence and residue composition were largely conserved (Table 2). The primary difference was observed at the C-terminal region, where an additional methoxy resonance appeared at δ_H 3.72 and δ_C 52.6. This signal was absent in **1** and indicated methyl esterification of the terminal carboxyl group. The assignment was supported by a key HMBC correlation from the methoxy protons to the carbonyl carbon of the terminal Gly residue, thereby locating the methoxy group at the C terminus. Thus, the spectroscopic data demonstrated that **2** shares the same amino acid sequence as **1** but contains a methyl-esterified Gly residue at the C terminus (Figures 2B and 3B). The overall structure of **2** was therefore assigned as the methyl ester analogue of **1**. Accordingly, marinoacrebol B (**2**) was identified as the C-terminal methyl ester derivative of marinoacrebol A (**1**).

Table 2. ^{1}H and ^{13}C NMR Spectroscopic Data for Marinoacrebols B–D (**2**–**4**) in MeOD.

Unit	Position	**2** [a]		**3** [a]		Unit	Position	**4** [b]	
		δ_C, Type	**δ_H, Mult [c] (*J* in Hz)**	**δ_C, Type**	**δ_H, Mult [c] (*J* in Hz)**			**δ_C, Type**	**δ_H, Mult [c] (*J* in Hz)**
Ac	1	173.4, C		173.5, C		Ac	1	173.4, C	
	2	23.4, CH_3	2.10, s	23.4, CH_3	2.10, s		2	23.4, CH_3	2.10, s
Aib[1]	NH		8.49 [d], s		8.48 [d], s	Aib[1]	NH		8.49, s
	1	178.6, C		178.7, C			1	178.6, C	
	2	57.4, C		57.4, C			2	57.4, C	
	3	24.3, CH_3	1.52 *, m	23.8, CH_3	1.54 *, m		3	26.1, CH_3	1.52 *, m
	4	27.0, CH_3	1.43, s	27.5, CH_3	1.51 *, m		4	26.8, CH_3	1.55 *, m
Ala[2]	NH		8.35, d (3.8)		8.34 [d], d (3.8)	Ala[2]	NH		8.35, m
	1	176.0, C		176.0, C			1	176.0, C	
	2	52.8, CH	3.97 *, m	52.8, CH	3.97 *, m		2	52.8, CH	3.97, m
	3	16.7, CH_3	1.14, d (7.4)	16.7, CH_3	1.15, d (7.4)		3	16.7, CH_3	1.14, d (7.5)
Phe[3]	NH		8.23, d (8.4)		8.23 [d], d (8.6)	Phe[3]	NH		8.23, d (8.5)
	1	174.1, C		174.1, C			1	174.0, C	
	2	56.9, CH	4.46 *, m	56.8, CH	4.50 *, m		2	56.1, CH	4.53 *, m
	3	38.0, CH_2	3.33 *, m; 3.13, dd (14.2, 11.9)	38.3, CH_2	3.31 *, m; 2.97, t (12.8)		3	38.1, CH_2	3.28 *, m; 3.05, t (12.6)
	4	139.0, C		139.2, C			4	139.6, C	
	5/5′	129.9, CH	7.25 *, m	130.3, CH	7.29 *, m		5/5′	130.5, CH	7.33 *, m
	6/6′	129.5, CH	7.23 *, m	129.6, CH	7.35 *, m		6/6′	129.6, CH	7.32 *, m
	7	127.8, CH	7.20 *, m	127.6, CH	7.21 *, m		7	127.6, CH	7.19 *, m
Iva[4]	NH		7.78, s		7.79, s	Iva[4]	NH		7.79, s
	1	174.6, C		174.3, C			1	176.2, C	
	2	60.6, C		60.6, C			2	60.6, C	
	3	29.9, CH_2	2.31, m; 1.93 *, m	30.3, CH_2	2.31 *, m; 1.92 *, m		3	29.9, CH_2	2.30 *, m; 1.91 *, m
	4	8.0, CH_3	0.94 *, m	8.0, CH_3	0.94 *, m		4	8.0, CH_3	0.95 *, m
	5	20.9, CH_3	1.58 *, m	20.5, CH_3	1.59 *, m		5	20.5, CH_3	1.59 *, m
Hyp[5]	OH	not obsd		not obsd		Hyp[5]	OH	not obsd	
	1	176.2, C		176.2, C			1	176.2, C	
	2	63.3, CH	4.57, m	63.3, CH	4.57, m		2	63.3, CH	4.56, t (9.1)
	3	38.1, CH_2	2.38 *, m; 1.83 *, m	38.1, CH_2	2.37 *, m; 1.83 *, m		3	38.1, CH_2	2.36 *, m; 1.82 *, m
	4	71.3, CH	4.46 *, m	71.3, CH	4.46 *, m		4	71.3, CH	4.45 *, m
	5	58.1, CH_2	3.87 *, m; 3.29 *, m	58.0, CH_2	3.90 *, m; 3.56 *, m		5	58.4, CH_2	3.88 *, m; 3.57 *, m

Table 2. *Cont.*

Unit	Position	2 [a]		3 [a]		Unit	Position	4 [b]	
		δ_C, Type	δ_H, Mult [c] (*J* in Hz)	δ_C, Type	δ_H, Mult [c] (*J* in Hz)			δ_C, Type	δ_H, Mult [c] (*J* in Hz)
Leu[6]	NH		7.97, d (7.1)		7.97, d (7.1)	Leu[6]	NH		7.98, d (7.1)
	1	175.9, C		175.9, C			1	175.9, C	
	2	55.7, CH	4.10 *, m	56.1, CH	4.10 *, m		2	55.7, CH	4.10 *, m
	3	40.4, CH_2	1.93 *, m	40.4, CH_2	1.94 *, m		3	40.4, CH_2	1.93 *, m
			1.64 *, m		1.64 *, m				1.63 *, m
	4	26.3, CH	1.82 *, m	26.3, CH	1.83 *, m		4	26.3, CH	1.82 *, m
	5	23.8, CH_3	1.06, d (6.6)	23.8, CH_3	1.06, d (6.6)		5	23.8, CH_3	1.06, d (6.6)
	6	21.5, CH_3	0.94 *, m	21.5, CH_3	0.94 *, m		6	21.5, CH_3	0.94 *, m
Aib[7]	NH		7.62, s		7.62, s	Aib[7]	NH		7.63, s
	1	177.6, C		177.6, C			1	177.6, C	
	2	57.8, C		57.8, C			2	57.8, C	
	3	23.9, CH_3	1.51 *, m	23.9, CH_3	1.50 *, m		3	23.9, CH_3	1.49 *, m
	4	26.9, CH_3	1.49 *, m	26.9, CH_3	1.58 *, m		4	27.1, CH_3	1.57 *, m
Aib[8]	NH		7.74, s		7.74, s	Aib[8]	NH		7.74, s
	1	178.6, C		178.6, C			1	178.6, C	
	2	57.8, C		57.7, C			2	57.8, C	
	3	23.9, CH_3	1.51 *, m	23.4, CH_3	1.51 *, m		3	23.3, CH_3	1.52 *, m
	4	26.9, CH_3	1.49 *, m	27.6, CH_3	1.55 *, m		4	27.6, CH_3	1.55 *, m
Ala[9]	NH		7.88, d (5.3)		7.90, d (5.2)	Ala[9]	NH		7.88, d (5.5)
	1	176.4, C		176.4, C			1	176.4, C	
	2	53.0, CH	4.16, dd (7.7, 5.6)	53.1, CH	4.16, dd (7.7, 5.4)		2	53.0, CH	4.16 *, m
	3	16.9, CH_3	1.59 *, m	16.9, CH_3	1.60 *, m		3	16.9, CH_3	1.59 *, m
Ala[10]	NH		8.06, d (7.4)		8.05, d (7.3)	Ala[10]	NH		8.07, d (7.0)
	1	175.7, C		176.0, C			1	175.7, C	
	2	51.4, CH	4.52 *, m	51.3, CH	4.53 *, m		2	51.4, CH	4.51 *, m
	3	17.7, CH_3	1.57 *, m	17.7, CH_3	1.55 *, m		3	17.8, CH_3	1.56 *, m
Iva[11]/Aib[11]	NH		7.81, s		7.93, s	Iva[11]	NH		7.79, s
	1	174.3, C		175.7, C			1	174.3, C	
	2	61.9, C		58.0, C			2	61.9, C	
	3	30.5, CH_2	2.25, m; 1.94, t (7.6)	24.2, CH_3	1.63 *, m		3	30.5, CH_2	2.23, m; 1.94 *, m
	4	8.6, CH_3	0.90 *, m	24.3, CH_3	1.59 *, m		4	8.6, CH_3	0.90 *, m
	5	24.5, CH_3	1.51 *, m				5	21.1, CH_3	1.51 *, m
Hyp[12]	OH	not obsd		not obsd		Hyp[12]	OH	not obsd	
	1	174.7, C		174.7, C			1	174.7, C	
	2	62.7, CH	4.40, t (8.9)	62.7, CH	4.40, t (8.9)		2	62.7, CH	4.39, t (9.0)
	3	37.7, CH_2	2.04 *, m; 0.99 *, m	37.7, CH_2	2.04 *, m; 0.99 *, m		3	37.6, CH_2	2.02 *, m; 0.96 *, m
	4	70.8, CH	4.22 *, m	70.8, CH	4.22 *, m		4	70.8, CH	4.20 *, m
	5	58.4, CH_2	3.88 *, m	58.4, CH_2	3.88 *, m		5	58.1, CH_2	3.87 *, m
			3.57, dd (12.8, 2.6);		3.57, dd (12.8, 2.6);				3.48 *, m
Phe[13]	NH		8.11 *, m		8.11 *, m	Phe[13]	NH		8.10, d (8.8)
	1	174.5, C		174.5, C			1	174.6, C	
	2	56.0, CH	4.50 *, m	56.0, CH	4.50 *, m		2	56.7, CH	4.44 *, m
	3	38.0, CH_2	3.35 *, m; 2.96, t (12.9)	38.0, CH_2	3.35 *, m; 3.13, dd (16.0, 11.6)		3	38.3, CH_2	3.26 *, m; 2.92, t (13.1)
	4	139.2, C		139.0, C			4	139.3, C	
	5/5′	130.3, CH	7.28 *, m	129.9, CH	7.34 *, m		5/5′	130.2, CH	7.26 *, m
	6/6′	129.6, CH	7.35 *, m	129.5, CH	7.25 *, m		6/6′	129.7, CH	7.34 *, m
	7	127.9, CH	7.22 *, m	127.8, CH	7.20 *, m		7	127.8, CH	7.21 *, m
Iva[14]	NH		7.56, s		7.55, s	Iva[14]	NH		7.52, s
	1	173.3, C		173.3, C			1	173.2, C	
	2	60.8, C		60.8, C			2	60.8, C	
	3	29.8, CH_2	2.32 *, m; 1.93 *, m	29.9, CH_2	2.35 *, m; 1.96 *, m		3	30.1, CH_2	2.29 *, m; 1.83 *, m
	4	8.0, CH_3	0.90 *, m	8.0, CH_3	0.94 *, m		4	8.0, CH_3	0.93 *, m
	5	20.5, CH_3	1.53 *, m	20.9, CH_3	1.52 *, m		5	21.0, CH_3	1.51 *, m

Table 2. *Cont.*

Unit	Position	2 [a]		3 [a]		Unit	Position	4 [b]	
		δ_C, Type	δ_H, Mult [c] (*J* in Hz)	δ_C, Type	δ_H, Mult [c] (*J* in Hz)			δ_C, Type	δ_H, Mult [c] (*J* in Hz)
Aib[15]	NH		8.13 *, m		7.96 *, m	Pro[15]	1	174.8, C	
	1	175.7, C		178.7, C			2	63.6, CH	4.42 *, m
	2	57.8, C		55.7, C			3	29.9, CH_2	2.02 *, m
	3	23.4, CH_3	1.60 *, m	23.8, CH_3	1.50 *, m				1.37 *, m
	4	26.8, CH_3	1.49 *, m	26.8, CH_3	1.43, s		4	26.4, CH_2	1.74 *, m
Pro[16]	1	175.3, C		175.2, C					1.68 *, m
	2	63.9, CH	4.69, t (7.4)	63.9, CH	4.68, dd (7.7, 6.8)		5	49.7, CH_2	3.74 *, m
	3	30.3, CH_2	2.34 *, m; 1.84 *, m	30.3, CH_2	2.35 *, m; 1.86 *, m	Aib[16]	NH		8.06, s
							1	176.3, C	
	4	27.0, CH_2	1.99 *, m; 1.92 *, m	27.0, CH_2	1.99 *, m; 1.94 *, m		2	58.2, C	
							3	23.8, CH_3	1.54 *, m
	5	50.2, CH_2	3.89 *, m; 3.54 *, m	50.2, CH_2	3.87 *, m; 3.54 *, m		4	24.5, CH_3	1.52 *, m
						Pro[17]	1	175.2, C	
mPro[17]	1	174.5, C		174.3, C			2	63.9, CH	4.68, t (7.3)
	2	64.8, CH	4.23 *, m	64.8, CH	4.23, m		3	30.3, CH_2	2.33 *, m;
	3	38.0, CH_2	2.36 *, m; 0.54, m	38.0, CH_2	2.13 *, m; 0.54, m				1.84 *, m
							4	26.9, CH_2	1.98 *, m;
	4	35.3, CH	2.14 *, m	35.3, CH	2.15 *, m				1.89 *, m
	5	16.6, CH_3	1.01, d (5.8)	16.5, CH_3	1.01, d (6.0)		5	50.0, CH_2	3.85 *, m;
	6	57.0, CH_2	3.99 *, m	57.0, CH_2	3.97 *, m;				3.52 *, m
Phe[18]	NH		8.12 *, m		8.12 *, m	Phe[18]	NH		8.03 *, m
	1	174.6, C		174.0, C			1	174.6, C	
	2	56.8, CH	4.50 *, m	56.1, CH	4.53 *, m		2	56.8, CH	4.51 *, m
	3	37.7, CH_2	3.40, dd (13.7, 3.6); 3.03, t (13.2)	37.8, CH_2	3.42 *, m; 3.04, t (13.1)		3	38.0, CH_2	3.33, m; 3.13, t (13.0)
	4	139.5, C		139.6, C			4	139.0, C	
	5/5′	130.5, CH	7.35 *, m	130.5, CH	7.32 *, m		5/5′	129.9, CH	7.24 *, m
	6/6′	129.7, CH	7.34 *, m	129.7, CH	7.30 *, m		6/6′	129.5, CH	7.24 *, m
	7	127.6, CH	7.20 *, m	127.9, CH	7.19 *, m		7	127.9, CH	7.18 *, m
Gly[19]	NH		7.95, t (6.0)		7.97 *, m				
	1	171.1, C		172.3, C					
	2	42.1, CH_2	3.99 *, m;	42.0, CH_2	3.95 *, m;				
	1-OMe	52.6, CH_3	3.72, s						

[a] 400 MHz for ^{1}H NMR and 100 MHz for ^{13}C NMR. [b] 900 MHz for ^{1}H NMR and 225 MHz for ^{13}C NMR. [c] Numbers of attached protons were determined by analysis of 2D spectra. [d] NH signals may be interchangeable. * Overlapped signals.

Marinoacrebol C (**3**) was also isolated as a white amorphous powder, and its molecular formula was determined to be $C_{97}H_{143}N_{19}O_{23}$ based on HR-ESI-MS data, which showed an $[M - H]^-$ ion at *m*/*z* 1941.0430 (calcd for $C_{97}H_{142}N_{19}O_{23}^-$, 1941.0531). The ^{1}H NMR spectrum displayed 15 exchangeable NH protons (δ_H 7.55–8.48) along with 13 α-proton signals (δ_H 3.95–4.68). The ^{13}C NMR and HSQC spectra revealed 97 carbon signals, including 20 carbonyl carbons (δ_C 172.3–178.7), indicating a 19-residue peptide (Table 2).

Detailed comparison of the NMR data of **3** with those of **1** revealed that the two compounds were highly similar, suggesting that only a localized structural change had occurred. Inspection of the aliphatic region showed the disappearance of the characteristic Iva[11] signals observed in **1**, namely the methyl and methylene resonances associated with the isovaline residue. Instead, **3** displayed resonances diagnostic of an Aib residue, including a quaternary carbon at δ_C 58.0 and two methyl groups at δ_C 24.3 and 24.2, with corresponding proton signals at δ_H 1.59 and 1.63. These features were consistent with replacement of Iva[11] by Aib. The assignment was further supported by key HMBC correlations from the methyl protons to the adjacent quaternary carbon and carbonyl carbon, establishing the identity of this residue as Aib. Because the remaining NMR data closely matched those of **1**, the remainder of the sequence was inferred to be unchanged. This conclusion was consistent with the

observed mass difference between **1** and **3**, which corresponded to the replacement of Iva by Aib. Based on these spectroscopic data, marinoacrebol C (**3**) was assigned as the Aib^{11} analogue of **1**, with the complete sequence *N*-Ac-Aib^{1}- Ala^{2}-Phe^{3}-Iva^{4}-Hyp^{5}-Leu^{6}-Aib^{7}-Aib^{8}-Ala^{9}-Ala^{10}-Aib^{11}-Hyp^{12}-Phe^{13}-Iva^{14}-Aib^{15}-Pro^{16}-mPro^{17}-Phe^{18}-Gly^{19} (Figures 2C and 3C). Therefore, marinoacrebol C (**3**) was identified as the Aib^{11} analogue of marinoacrebol A (**1**) (Figures S18–S23).

Marinoacrebol D (**4**) was isolated as a pale pink amorphous powder, with a molecular formula of $C_{95}H_{140}N_{18}O_{22}$ based on HR-ESI-MS data, which showed an $[M + Na]^+$ ion at m/z 1908.0195 (calcd for $C_{95}H_{140}N_{18}NaO_{22}{}^+$, 1908.0282). Compared with **1**, both the molecular formula and NMR data suggested that **4** is a shortened analogue containing one fewer nitrogen atom and fewer carbons overall, consistent with a reduced peptide length. The ^{11}H NMR spectrum displayed 14 exchangeable NH protons (δ_H 7.52–8.49) along with 11 α-proton signals (δ_H 3.97–4.68). The ^{13}C NMR and HSQC spectra revealed 95 carbon signals, including 19 carbonyl carbons (δ_C 173.2–178.6), supporting the assignment of **4** as an 18-residue peptide (Table 2).

Analysis of the 2D NMR and ESI-MS/MS data indicated that the N-terminal portion of **4** is identical to that of **1**, extending from the N-acetyl group through Iva^{14}. Therefore, the structural divergence was localized to the C-terminal region. In place of the Aib^{15}-Pro^{16}-mPro^{17}-Phe^{18}-Gly^{19} sequence present in **1**, compound **4** was shown to possess a modified terminal segment composed of Pro^{15}-Aib^{16}-Pro^{17}-Phe^{18}. This revised assignment was supported by key HMBC correlations: H-5 of Pro^{15} showed a correlation with the carbonyl carbon of Iva^{14}, establishing the Iva^{14}–Pro^{15} linkage; the NH of Aib^{16} showed a correlation with the carbonyl carbon of Pro^{15}, confirming the Pro^{15}–Aib^{16} linkage; and H-5 of Pro^{17} showed a correlation with the carbonyl carbon of Aib^{16}, supporting the Aib^{16}-Pro^{17} linkage (Figures S26–S31). The remaining Pro^{17}–Phe^{18} connection was corroborated by the MS/MS fragmentation pattern, which was consistent with the proposed C-terminal sequence. Taken together, these data established **4** as an 18-residue analogue of **1** featuring truncation of the terminal Gly residue and rearrangement of the final peptide segment. Thus, marinoacrebol D (**4**) was assigned as an 18-residue peptide featuring the modified C-terminal sequence Pro^{15}-Aib^{16}-Pro^{17}-Phe^{18} (Figures 2D and 3D).

2.2. Absolute Configurations of Compounds **1**–**4**

The absolute configurations of the amino acid residues in marinoacrebols A–D (**1**–**4**) were determined by acid hydrolysis followed by advanced Marfey's method. The hydrolysates were derivatized with L-FDLA (1-fluoro-2,4-dinitrophenyl-5-l-leucineamide), D-FDLA, and a mixture of L- and D-FDLA, and the resulting derivatives were analyzed by LC-ESI-MS. The configurations were assigned by comparing the retention times of the derivatives with those of corresponding amino acid standards. Marfey's analysis of **1**–**4** showed that the amino acid residues shared the same absolute configurations among the four compounds. Ala, Phe, Hyp, Leu, Pro, and mPro were assigned to the L-configuration, whereas Iva was assigned to the D-configuration (Figures S34–S38). Aib and Gly were identified as achiral residues. In particular, the absolute configurations of Hyp and mPro were initially assigned as L-forms based on comparison with derivatives prepared using a mixture of L- and D-FDLA reagents.

To further establish the stereochemistry of these residues, authentic *cis*- and *trans*-L-Hyp as well as *cis*- and *trans*-L-mPro standards were derivatized and analyzed under identical LC conditions. The L-FDLA derivatives of *trans*-L-Hyp and *cis*-L-Hyp were observed at 28.09 and 30.03 min, respectively, whereas those of *cis*-L-mPro and *trans*-L-mPro eluted at 38.03 and 38.75 min, respectively. The L-FDLA derivatives of peptide-derived Hyp and mPro eluted at 28.09 and 37.82 min, respectively, matching the retention times of the corresponding

standards and identifying these residues as *trans*-L-Hyp and *cis*-L-mPro (Figure S34). In addition, the electronic circular dichroism (ECD) spectra of compounds **1**–**4** exhibited a positive Cotton effect at 196 nm and negative Cotton effects at 211 and 226 nm, consistent with a right-handed helical conformation (Figure 4).

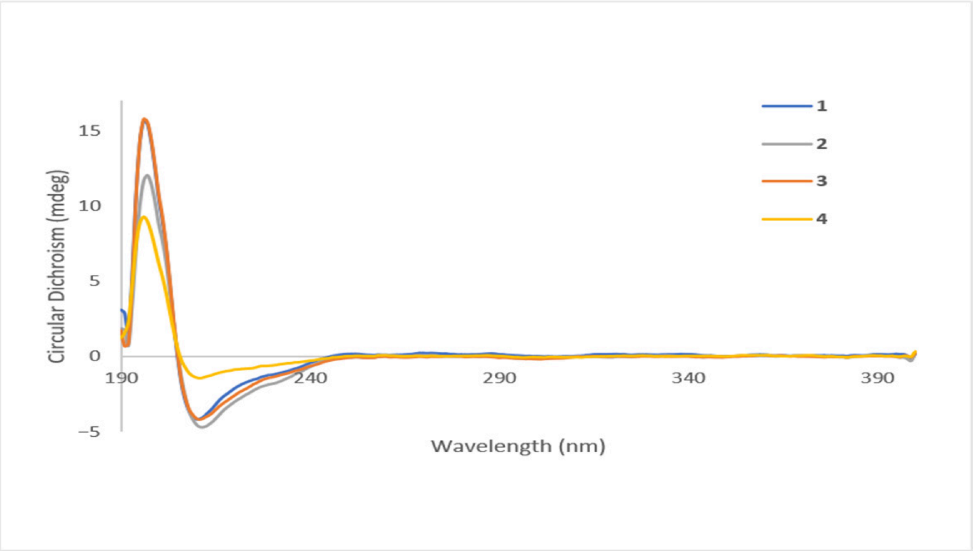

Figure 4. ECD spectrum of compounds **1**–**4** in methanol.

Marinoacrebols A–D (**1**–**4**) were identified as linear peptaibol-like peptides based on their characteristic structural features, including the presence of the nonproteinogenic amino acids such as Aib and Iva, an N-terminal acetyl group, and peptide backbones comprising 18–19 amino acid residues. However, compounds **1**–**4** differ in their C-terminal functionalities, with three compounds bearing a carboxylic acid group and one possessing a methyl ester group. Considering their overall structural similarities to previously reported peptaibols, compounds **1**–**4** are described as peptaibol-like peptides. These structural characteristics are consistent with those of previously reported peptaibols, which are generally biosynthesized by nonribosomal peptide synthetases (NRPSs) [13,14]. Peptaibols have been extensively studied, particularly those produced by terrestrial fungi such as *Trichoderma* spp., with representative compounds such as alamethicin exhibiting well-defined helical conformations and voltage-dependent ion-conducting channel activity in lipid bilayers [19,20].

Compared with these well-characterized peptaibols, marinoacrebols A–D display both conserved and distinctive structural features. Although their peptide lengths fall within the typical range reported for peptaibols, their amino acid composition shows notable differences. In particular, the coexistence of multiple Aib residues with Iva, together with the simultaneous presence of Hyp and mPro, represents a relatively uncommon structural combination among reported peptaibols. Aib residues are well known to favor helical conformations in peptaibols, whereas proline and hydroxyproline residues can introduce local conformational constraints into peptide backbones [14,19]. Thus, the particular distribution of Aib, Hyp, and mPro residues in marinoacrebols may influence their conformational properties, although detailed conformational studies will be required to establish their three-dimensional structures and structure–activity relationships.

The structural characteristics of marinoacrebols A–D are consistent with their likely origin from an NRPS-mediated biosynthetic pathway. NRPS systems possess modular architectures that enable the incorporation of both proteinogenic and nonproteinogenic amino acids and frequently generate families of structurally related peptide metabolites.

The structural variations observed among compounds **1**–**4**, including the Iva/Aib variation, differences in C-terminal modification, and peptide truncation, are therefore compatible with the microheterogeneity commonly encountered among fungal peptaibols. Such structural variations may plausibly arise from the substrate flexibility and product diversity generally associated with fungal NRPS systems [13,16]. Accordingly, the observed differences among marinoacrebols are discussed here as structural variations consistent with established patterns of peptaibol biosynthesis rather than as evidence for specific enzymatic mechanisms.

The production of several closely related marinoacrebol analogues by a single *Acremonium* strain further highlights the structural microheterogeneity characteristic of many fungal peptaibol families. Such diversity is consistent with the variable amino acid incorporation and structural variation frequently reported for NRPS-derived peptaibols [13,14,16]. Although the biological significance of this structural variation remains to be established, the occurrence of multiple analogues expands the chemical diversity of the marinoacrebol family and provides a basis for future studies examining relationships among sequence variation, peptide conformation, and biological activity.

2.3. Antibacterial Activity

Compounds **1**–**4** were evaluated for antibacterial activity against three Gram-positive bacteria, *Bacillus subtilis* KCTC 1021, *Kocuria rhizophila* KCTC 1915, and *Staphylococcus aureus* KCTC 1621, as well as three Gram-negative bacteria, *Escherichia coli* KCTC 2441, *Salmonella typhimurium* KCTC 2515, and *Klebsiella pneumoniae* KCTC 2690. Compounds **1**–**4** exhibited selective antibacterial activity against Gram-positive bacteria, with minimum inhibitory concentration (MIC) values of 16–32 μg/mL against *B. subtilis*, 8–32 μg/mL against *K. rhizophila*, and 32–64 μg/mL against *S. aureus*. In particular, **2** exhibited the most potent activity against *K. rhizophila*, with an MIC of 8 μg/mL, whereas the other compounds exhibited activities within similar ranges. In contrast, none of the compounds exhibited detectable activity against the tested Gram-negative bacteria (Table 3).

Table 3. Antibacterial Activity (MIC, μg/mL) of Compounds **1**–**4**.

Compounds	Minimal Inhibitory Concentration (μg/mL; μM)					
	Gram (+) Bacteria			Gram (−) Bacteria		
	B. subtilis **KCTC 1021**	***K. rhizophila*** **KCTC 1915**	***S. aureus*** **KCTC 1621**	***E. coli*** **KCTC 2441**	***S. typhimurium*** **KCTC 2515**	***K. pneumoniae*** **KCTC 2690**
1	16; 8.18	32; 16.36	64; 32.72	>128; 65.44	>128; 65.44	>128; 65.44
2	16; 8.12	8; 4.06	32; 16.24	>128; 64.97	>128; 64.97	>128; 64.97
3	32; 16.48	32; 16.48	32; 16.48	>128; 65.91	>128; 65.91	>128; 65.91
4	32; 16.98	32; 16.98	32; 16.98	>128; 67.90	>128; 67.90	>128; 67.90
Ampicillin	0.5; 1.43	0.25; 0.72	2; 5.72	64; 183.19	16; 45.80	>128; 366.30
Vancomycin	0.25; 0.17	0.25; 0.17	0.25; 0.17	>128; 88.32	>128; 88.32	>128; 88.32

Previous studies have shown that structural variations can influence the antibacterial activity of peptaibols. For example, amino acid substitutions in *Acremonium*-derived emerimicins markedly affected their antibacterial activity [21]. In addition, methyl ester derivatives have been reported to exhibit higher antimicrobial activity than their counterparts bearing free carboxylic groups, potentially owing to their lower polarity and improved membrane penetration [22]. Although this finding was reported for a different chemical scaffold, it suggests that changes in terminal functionality and physicochemical properties may contribute to differences in antimicrobial activity. Such structural effects may also be

relevant to the relatively high activity of compound **2** against *K. rhizophila*, although further studies are required to clarify the underlying mechanism.

3. Materials and Methods

3.1. General Experimental Procedures

Optical rotations were measured using a Krüss Optronic P-8000 polarimeter with a 5-cm cell (Krüss, Hamburg, Germany) in methanol (MeOH). UV spectra were acquired using a Varian Cary 50 UV–vis spectrophotometer (Varian Inc., Mulgrave, Australia). ECD spectra were obtained using a JASCO J-810 spectrometer (JASCO Inc., Tokyo, Japan) in MeOH at a compound concentration of 0.1 mg/mL using a quartz cuvette with an optical path length of 10 mm. IR spectra were recorded using a Thermo Fisher Scientific Nicolet iS 10 Fourier-transform infrared (FT-IR) spectrometer (Waltham, MA, USA). The weak absorption observed around 2200–2400 cm^{-1} was also present in the $CHCl_3$ blank spectrum and was therefore attributed to background signals rather than to the samples. NMR spectra were recorded using an Agilent 400-MR DD2 spectrometer (Agilent Technologies, Santa Clara, CA, USA) operating at 400 MHz for ^1H and 100 MHz for ^{13}C at the Ewha Drug Development Research Core Center, and a Bruker Avance Neo 900 MHz NMR spectrometer operating at 900 MHz for ^1H and 225 MHz for ^{13}C and equipped with a TCi cryogenic probe. NMR spectra were recorded in methanol-d_4 (MeOD) using the solvent signals as references (δ_H 3.31 ppm and δ_C 49.0 ppm). Low-resolution LC-MS measurements were performed using an Agilent 1260 quadrupole LC-MS system (Agilent Technologies, Santa Clara, CA, USA) and a Waters Alliance Micromass ZQ LC-MS system (Waters Corp., Milford, MA, USA), equipped with a reversed-phase Phenomenex Luna C18(2) column (100 Å, 100 mm × 4.6 mm, 5 µm; Phenomenex, Torrance, CA, USA), at a flow rate of 1.0 mL/min at the National Research Facilities and Equipment Center (NanoBioEnergy Materials Center), Ewha Womans University. High-resolution ESI-MS (HR-ESI-MS) spectra were acquired using an Agilent 6230 TOF LC-MS system (Agilent Technologies, Santa Clara, CA, USA) at the Ewha Drug Development Research Core Center and a UHPLC Xevo G3 QToF mass spectrometer system (Waters, Milford, MA, USA) at the College of Pharmacy, Seoul National University. Column chromatography was performed using reversed-phase C18 gel (70–230 mesh; Merck, Darmstadt, Germany) with a stepwise gradient of water and methanol. Fractions were purified by reversed-phase HPLC using a Phenomenex Luna C18(2) column (250 × 10 mm, 5 µm, 100 Å) at a flow rate of 2.0 mL/min. ESI-MS/MS analyses were conducted using a Thermo Scientific Q Exactive Plus mass spectrometer (NFEC-2021-01-267431) at the Core Research Center for Natural Products and Medicinal Materials (CRCNM), Yeungnam University, and a Thermo Scientific LTQ XL linear ion trap mass spectrometer coupled with a Vanquish UHPLC system (Thermo Fisher Scientific, Waltham, MA, USA) at the Natural Products Research Institute, Seoul National University.

3.2. Strain ACE-015 Collection and Strain Isolation

Strain ACE-015, a marine-derived fungus, was obtained from the National Marine Biodiversity Institute of Korea (MBRIS) under accession number SFC20190314-M01. According to the information proved by MBRIS, the strain was originally collected in Jung-gu, Incheon, South Korea (37°27′44.6″ N, 126°29′49.8″ E) and was identified as *Acremonium persicinum*.

3.3. Cultivation, Extraction and Purification

Strain ACE-015 was cultivated in thirty-six 2.5 L Ultra Yield Flasks, each containing 1 L of production medium composed of potato dextrose broth (24 g/L) and artificial sea salt (34.75 g/L) dissolved in distilled water. The cultures were incubated at 27 °C with shaking at 120 rpm for 7 days. After fermentation, the entire culture broth was extracted

with ethyl acetate. The organic layer was concentrated under reduced pressure to yield 6.4 g of crude extract. The crude extract was fractionated by reversed-phase C18 column chromatography using a stepwise gradient of H_2O/MeOH mixtures (80:20, 60:40, 50:50, 40:60, 30:70, 20:80, 0:100, and 0:100; 100 mL each), yielding eight fractions (F1–F8). Fraction F6 (1.82 g) was further separated by reversed-phase C18 column chromatography using a finer step-gradient elution with H_2O/MeOH mixtures (30:70, 25:75, 20:80, 15:85, 10:90, 5:95, and 0:100; 100 mL each) to afford seven subfractions (F6.1–F6.7). Subfraction F6.3 (231.3 mg) was purified by reversed-phase HPLC using a Phenomenex Luna C18(2) column (250 × 10 mm, 5 µm, 100 Å) under isocratic conditions with 58% CH_3CN in H_2O containing 0.1% trifluoroacetic acid (TFA) at a flow rate of 2.0 mL/min, with UV detection at 210 nm, to afford F6.3-5 (8.7 mg), F6.3-7 (7.4 mg), and F6.3-8 (36.8 mg). F6.3-8 (36.8 mg) was purified by reversed-phase HPLC using a Phenomenex Luna C18(2) column (250 × 10 mm, 5 µm, 100 Å) with 86% aqueous MeOH containing 0.1% TFA under isocratic conditions at a flow rate of 2.0 mL/min, with UV detection at 210 nm, to obtain marinoacrebol A (**1**, 11.1 mg, t_R = 42.6 min) and marinoacrebol B (**2**, 5.8 mg, t_R = 51.0 min). F6.3-7 (7.4 mg) was purified by reversed-phase HPLC using a Phenomenex Luna C18(2) column (250 × 10 mm, 5 µm, 100 Å) with 85% aqueous MeOH containing 0.1% TFA under isocratic conditions at a flow rate of 2.0 mL/min, with UV detection at 210 nm, to yield marinoacrebol C (**3**, 2.3 mg, t_R = 51.8 min). F6.3-5 (8.7 mg) was purified under the same HPLC conditions using 65% aqueous CH_3CN containing 0.1% TFA to yield marinoacrebol D (**4**, 3.4 mg, t_R = 30.7 min).

Marinoacrebol A (**1**): white amorphous solid; $[\alpha]_D^{21}$: −18.4 (*c* 0.01, MeOH); UV (MeOH) λmax (log ε) 208 (2.47) nm; ECD (*c* 5.11 × 10^{-5} M, MeOH); IR (KBr) *ν*max 3289, 2955, 2924, 2854, 1645, 1456, and 668 cm^{-1}; ^1H and ^{13}C NMR data (900 and 225 MHz, MeOD), Table 1; LR-ESI-MS *m*/*z* 1958.11 $[M + H]^+$; HR-ESI-MS *m*/*z* 1955.0595 $[M - H]^-$ (calcd for $C_{98}H_{144}N_{19}O_{23}^-$, 1955.0688).

Marinoacrebol B (**2**): white amorphous solid; $[\alpha]_D^{21}$: +33.6 (*c* 0.01, MeOH); UV (MeOH) λmax (log ε) 204 (2.03) nm; ECD (*c* 5.08 × 10^{-5} M, MeOH); IR (KBr) *ν*max 3272, 2929, 1645, 1539, 1456, 1204, and 757 cm^{-1}; ^1H and ^{13}C NMR data (400 and 100 MHz, MeOD), Table 2; LR-ESI-MS *m*/*z* 1993.09 $[M + Na]^+$; HR-ESI-MS *m*/*z* 1969.0777 $[M - H]^-$ (calcd for $C_{99}H_{146}N_{19}O_{23}^-$, 1969.0844).

Marinoacrebol C (**3**): white amorphous solid; $[\alpha]_D^{21}$: +83.2 (*c* 0.01, MeOH); UV (MeOH) λmax (log ε) 202 (2.43) nm; ECD (*c* 5.15 × 10^{-5} M, MeOH); IR (KBr) *ν*max 3281, 2956, 2922, 2850, 1644, 1463, and 761 cm^{-1}; ^1H and ^{13}C NMR data (400 and 100 MHz, MeOD), Table 2; LR-ESI-MS *m*/*z* 1965.38 $[M + Na]^+$; HR-ESI-MS *m*/*z* 1941.0430 $[M - H]^-$ (calcd for $C_{97}H_{142}N_{19}O_{23}^-$, 1941.0531).

Marinoacrebol D (**4**): pale pink amorphous solid; $[\alpha]_D^{21}$: −20.8 (*c* 0.01, MeOH); UV (MeOH) λmax (log ε) 200 (2.58) nm; ECD (*c* 5.31 × 10^{-5} M, MeOH); IR (KBr) *ν*max 3291, 2925, 2853, 1648, 1458, 1202, and 761 cm^{-1}; ^1H and ^{13}C NMR data (900 and 225 MHz, MeOD), Table 2; LR-ESI-MS *m*/*z* 1908.03 $[M + Na]^+$; HR-ESI-MS *m*/*z* 1908.0195 $[M + Na]^+$ (calcd for $C_{95}H_{140}N_{18}NaO_{22}^+$, 1908.0282).

3.4. ESI-MS/MS Analysis

Each peptide was dissolved in methanol at a concentration of 0.3 mg/mL and introduced into a Thermo Scientific Q Exactive Plus mass spectrometer by direct infusion at an injection rate of 5 µL/min. MS experiments were performed in positive electrospray ionization mode using a spray voltage of 3.5 kV and a capillary temperature of 300 °C for compounds **1** and **4**, or a spray voltage of 3.0 kV and a capillary temperature of 250 °C for compounds **2** and **3**. The sheath gas flow rate was 7 AU, and the mass range was *m*/*z* 150–2000. The sodium adduct was selected as the precursor ion, and normalized collision energies (NCE) of 30, 35, and 40 were used for the MS/MS experiments to generate y_n-

and b_n-type fragments. Compounds **1**–**4** were also analyzed using a Thermo Scientific LTQ XL linear ion trap mass spectrometer coupled with a Vanquish UHPLC system. MS/MS experiments were performed in positive electrospray ionization mode with a spray voltage of 3.47 kV, a capillary temperature of 320 °C, and a capillary voltage of 10.97 V. Data were acquired in full-scan mode. The precursor ion was fragmented at a collision energy of 35.0 eV to generate y_n- and b_n-type fragments.

3.5. Acid Hydrolysis and Advanced Marfey's Analysis

The absolute configurations of the amino acid residues in marinoacrebols A–D (**1**–**4**) were determined using Marfey's method following acid hydrolysis. Each compound was hydrolyzed with 6 *N* HCl at 110 °C for 12 h. After removal of the solvent under reduced pressure, the resulting hydrolysate was dissolved in 1 *N* $NaHCO_3$ to adjust the solution to neutral conditions prior to derivatization. The hydrolysate, together with L- and D-amino acid standards, was derivatized with L-FDLA (1-fluoro-2,4-dinitrophenyl-5-L-leucineamide), D-FDLA, and a mixture of L- and D-FDLA in acetone at 60 °C for 1 h. The derivatization reaction was terminated by the addition of 2 *N* HCl and acetonitrile, and the resulting mixtures were analyzed by LC-ESI-MS. The absolute configurations of the amino acid residues were established by comparing the retention times of the derivatized hydrolysates with those of the corresponding derivatized standards. LC-ESI-MS analyses were performed on a Waters Micromass ZQ LC-MS system (Waters Corp., Milford, MA, USA) equipped with a Phenomenex Luna C18(2) reversed-phase column (100 Å, 100 mm × 4.6 mm, 5 µm; Phenomenex, Torrance, CA, USA), using gradient elution from 10% to 100% CH_3CN in H_2O containing 0.1% formic acid at a flow rate of 1.0 mL/min.

3.6. Antibacterial Activity Assay

The antibacterial activities of the isolated compounds were evaluated against six bacterial strains: *Escherichia coli* (KCTC 2441), *Salmonella typhimurium* (KCTC 2515), *Klebsiella pneumoniae* (KCTC 2690), *Bacillus subtilis* (KCTC 1021), *Kocuria rhizophila* (KCTC 1915), and *Staphylococcus aureus* (KCTC 1621). The bacteria were cultured overnight in Mueller–Hinton broth (MHB) at 37 °C and adjusted to a 0.5 McFarland standard (1.0×10^8 CFU/mL), followed by dilution to a final inoculum concentration of 5.0×10^5 CFU/mL. Test compounds and positive controls (ampicillin and vancomycin) were dissolved in dimethyl sulfoxide (DMSO) at 10 mg/mL and further diluted in MHB to 256 µg/mL. A 100 µL aliquot of each sample was added to the first column of a sterile 96-well microtiter plate and serially diluted twofold across the plate to obtain final concentrations ranging from 0.25–128 µg/mL. Subsequently, 50 µL of bacterial suspension was added to each well, resulting in final compound concentrations of 128–0.25 µg/mL and a final inoculum concentration of 5.0×10^5 CFU/mL. The final DMSO concentration in the compound-containing wells ranged from 1.28% to 0.0025% (*v*/*v*). MHB alone was used as the medium control, and MHB containing DMSO was used as the solvent control. The plates were incubated at 37 °C for 18–24 h under static conditions. The MIC was defined as the lowest compound concentration that completely inhibited visible bacterial growth and was confirmed by measuring absorbance at 600 nm using a SpectraMax® ABS Plus microplate reader (Molecular Devices, San Jose, CA, USA). All assays were performed in triplicate.

Supplementary Materials: The following supporting information can be downloaded at https://www.mdpi.com/article/10.3390/md24110402/s1, Figure S1: ^{1}H NMR Spectrum of Marinoacrebol A (**1**) in MeOD; Figure S2: ^{13}C NMR Spectrum of Marinoacrebol A (**1**) in MeOD; Figure S3: DEPT NMR Spectrum of Marinoacrebol A (**1**) in MeOD; Figure S4: COSY NMR Spectrum of Marinoacrebol A (**1**) in MeOD; Figure S5: HSQC NMR Spectrum of Marinoacrebol A (**1**) in MeOD; Figure S6: HMBC NMR Spectrum of Marinoacrebol A (**1**) in MeOD; Figure S7: High Resolution Mass Data of Marinoacrebol A (**1**); Figure S8: ESI-MS/MS spectrum of Marinoacrebol A (**1**); Figure S9: FT-IR Spectrum of Marinoacrebol A (**1**); Figure S10: ^{1}H NMR Spectrum of Marinoacrebol B (**2**) in MeOD; Figure S11: ^{13}C NMR Spectrum of Marinoacrebol B (**2**) in MeOD; Figure S12: COSY NMR Spectrum of Marinoacrebol B (**2**) in MeOD; Figure S13: HSQC NMR Spectrum of Marinoacrebol B (**2**) in MeOD; Figure S14: HMBC NMR Spectrum of Marinoacrebol B (**2**) in MeOD; Figure S15: High Resolution Mass Data of Marinoacrebol B (**2**); Figure S16: ESI-MS/MS spectrum of Marinoacrebol B (**2**); Figure S17: FT-IR Spectrum of Marinoacrebol B (**2**); Figure S18: ^{1}H NMR Spectrum of Marinoacrebol C (**3**) in MeOD; Figure S19: ^{13}C NMR Spectrum of Marinoacrebol C (**3**) in MeOD; Figure S20: COSY NMR Spectrum of Marinoacrebol C (**3**) in MeOD; Figure S21: HSQC NMR Spectrum of Marinoacrebol C (**3**) in MeOD; Figure S22: HMBC NMR Spectrum of Marinoacrebol C (**3**) in MeOD; Figure S23: High Resolution Mass Data of Marinoacrebol C (**3**); Figure S24: ESI-MS/MS spectrum of Marinoacrebol C (**3**); Figure S25: FT-IR Spectrum of Marinoacrebol C (**3**); Figure S26: ^{1}H NMR Spectrum of Marinoacrebol D (**4**) in MeOD; Figure S27: ^{13}C NMR Spectrum of Marinoacrebol D (**4**) in MeOD; Figure S28: COSY NMR Spectrum of Marinoacrebol D (**4**) in MeOD; Figure S29: HSQC NMR Spectrum of Marinoacrebol D (**4**) in MeOD; Figure S30: HMBC NMR Spectrum of Marinoacrebol D (**4**) in MeOD; Figure S31: High Resolution Mass Data of Marinoacrebol D (**4**); Figure S32: ESI-MS/MS spectrum of Marinoacrebol D (**4**); Figure S33: FT-IR Spectrum of Marinoacrebol D (**4**); Figure S34: Advanced Marfey's analysis of the amino acid residues from Marinoacrebol A (**1**); Figure S35: Co-injection analysis of the derivatized hydrolysate of Marinoacrebol A (**1**) with the corresponding amino acid standards; Figure S36: Advanced Marfey's analysis of the amino acid residues from Marinoacrebol B (**2**); Figure S37: Advanced Marfey's analysis of the amino acid residues from Marinoacrebol C (**3**); Figure S38: Advanced Marfey's analysis of the amino acid residues from Marinoacrebol D (**4**).

Author Contributions: D.C. and A.N.M. contributed equally to this work. Conceptualization, J.Y.L.; methodology, investigation, and writing—original draft preparation, D.C. and E.-Y.L.; compound isolation, D.C. and J.Y.L.; structure elucidation, D.C., E.-Y.L., H.-S.C., S.-Y.K., M.-J.J., H.K., S.-Y.S. and S.-S.C.; Advanced Marfey's analysis, E.-Y.L.; MS/MS analysis, Y.S.P. and A.N.M.; fungal strain isolation, G.C.; writing—review and editing, D.C., A.N.M., E.-Y.L., Y.S.P., J.-W.N., S.-Y.S., S.-S.C., S.H.S. and S.L.; supervision and project administration, H.C. and S.-J.N. All authors have read and agreed to the published version of the manuscript.

Funding: This research was supported by the National Research Foundation of Korea (NRF) grant funded by the Korea Government (MSIT) (RS-2024-00440614), by the Korea Institute of Marine Science & Technology Promotion (KIMST) funded by Ministry of Oceans and Fisheries (No. RS-2021-KS211520), by Basic Science Research Program through the National Research Foundation of Korea (NRF) funded by the Ministry of Education (RS-2021-NR060138), National Research Foundation of Korea grants funded by the Republic of Korean Government (Ministry of Science and ICT) (RS-2026-25480650, RS-2020-NR049591, RS-2025-02317758) and by 2024 Yeungnam University Research Grant funded by Yeungnam University, and Basic Science Research Program through the National Research Foundation of Korea (NRF) funded by the Ministry of Education (RS-2025-25397599).

Institutional Review Board Statement: Not applicable.

Data Availability Statement: The data supporting the findings of this study are provided in the manuscript and its Supporting Information.

Acknowledgments: We gratefully acknowledge Ewha Womans University for providing research support.

Conflicts of Interest: The authors declare no conflicts of interest.

Abbreviations

The following abbreviations are used in this manuscript:

COSY	Correlated spectroscopy
DEPT	Distortionless enhancement by polarization transfer
ECD	Electronic circular dichroism
ESI	Electrospray ionization
FDLA	1-Fluoro-2,4-dinitrophenyl-5-L-leucineamide
HMBC	Heteronuclear multiple bond correlation
HPLC	High-performance liquid chromatography
HSQC	Heteronuclear single-quantum correlation
MIC	Minimum inhibitory concentration
NMR	Nuclear magnetic resonance
NRPs	Nonribosomal peptides
NRPSs	Nonribosomal peptide synthetases
PDB	Potato dextrose broth
RiPPs	Ribosomally synthesized and post-translationally modified peptides
TFA	Trifluoroacetic acid
UV	Ultraviolet

References

1. Blunt, J.W.; Copp, B.R.; Keyzers, R.A.; Munro, M.H.G.; Prinsep, M.R. Marine natural products. *Nat. Prod. Rep.* **2018**, *35*, 8–53. [CrossRef] [PubMed]
2. Carroll, A.R.; Copp, B.R.; Davis, R.A.; Keyzers, R.A.; Prinsep, M.R. Marine natural products. *Nat. Prod. Rep.* **2020**, *37*, 175–223. [CrossRef] [PubMed]
3. Imhoff, J.F. Natural products from marine fungi—Still an underrepresented resource. *Mar. Drugs* **2016**, *14*, 19. [CrossRef] [PubMed]
4. Rateb, M.E.; Ebel, R. Secondary metabolites of fungi from marine habitats. *Nat. Prod. Rep.* **2011**, *28*, 290–344. [CrossRef] [PubMed]
5. Summerbell, R.C.; Gueidan, C.; Schroers, H.-J.; de Hoog, G.S.; Starink, M.; Rosete, Y.A.; Guarro, J.; Scott, J.A. Acremonium phylogenetic overview. *Stud. Mycol.* **2011**, *68*, 139–162. [CrossRef] [PubMed]
6. Tian, J.; Lai, D.; Zhou, L. Secondary metabolites from *Acremonium* fungi: Diverse structures and bioactivities. *Mini-Rev. Med. Chem.* **2017**, *17*, 603–632. [CrossRef] [PubMed]
7. Bugni, T.S.; Ireland, C.M. Marine-derived fungi: A chemically and biologically diverse group of microorganisms. *Nat. Prod. Rep.* **2004**, *21*, 143–163. [CrossRef] [PubMed]
8. Debbab, A.; Aly, A.H.; Proksch, P. Bioactive secondary metabolites from endophytes and associated marine fungi. *Fungal Divers.* **2011**, *49*, 1–12. [CrossRef]
9. Suciati; Fraser, J.A.; Lambert, L.K.; Pierens, G.K.; Bernhardt, P.V.; Garson, M.J. Secondary metabolites of the sponge-derived fungus *Acremonium persicinum*. *J. Nat. Prod.* **2013**, *76*, 1432–1440. [CrossRef] [PubMed]
10. He, H.; Bigelis, R.; Solum, E.H.; Greenstein, M.; Carter, G.T. Acremonidins, new polyketide-derived antibiotics produced by *Acremonium* sp. LL-Cyan 416. *J. Antibiot.* **2003**, *56*, 923–930. [CrossRef] [PubMed]
11. Sassa, T.; Ooi, T.; Kinoshita, H.; Okada, K. Absolute stereochemistry of acremolactone A, a novel herbicidal epoxydihydropyranyl γ-lactone from *Acremonium roseum* I4267. *Biosci. Biotechnol. Biochem.* **2004**, *68*, 2201–2204. [CrossRef] [PubMed]
12. Newman, D.J.; Cragg, G.M. Natural products as sources of new drugs over the nearly four decades from 01/1981 to 09/2019. *J. Nat. Prod.* **2020**, *83*, 770–803. [CrossRef] [PubMed]
13. Walsh, C.T.; Fischbach, M.A. Natural products version 2.0: Connecting genes to molecules. *J. Am. Chem. Soc.* **2010**, *132*, 2469–2493. [CrossRef] [PubMed]
14. Hou, X.; Sun, R.; Feng, Y.; Zhang, R.; Zhu, T.; Che, Q.; Zhang, G.; Li, D. Peptaibols: Diversity, bioactivity, and biosynthesis. *Eng. Microbiol.* **2022**, *2*, 100026. [CrossRef] [PubMed]
15. Dalla Torre, C.; Sannio, F.; Battistella, M.; Docquier, J.D.; De Zotti, M. Peptaibol analogs show potent antibacterial activity against multidrug resistant opportunistic pathogens. *Int. J. Mol. Sci.* **2023**, *24*, 7997. [CrossRef] [PubMed]
16. Süssmuth, R.D.; Mainz, A. Nonribosomal peptide synthesis—Principles and prospects. *Angew. Chem. Int. Ed.* **2017**, *56*, 3770–3821. [CrossRef] [PubMed]
17. Raaijmakers, J.M.; De Bruijn, I.; Nybroe, O.; Ongena, M. Natural functions of lipopeptides from *Bacillus* and *Pseudomonas*: More than surfactants and antibiotics. *FEMS Microbiol. Rev.* **2010**, *34*, 1037–1062. [CrossRef] [PubMed]
18. Raghothama, S. NMR of peptides. *J. Indian Inst. Sci.* **2010**, *90*, 145–166.

19. Szekeres, A.; Leitgeb, B.; Kredics, L.; Antal, Z.; Hatvani, L.; Manczinger, L.; Vágvölgyi, C. Peptaibols and related peptaibiotics of *Trichoderma*. *Acta Microbiol. Immunol. Hung.* **2005**, *52*, 137–168. [CrossRef] [PubMed]
20. Chugh, J.K.; Wallace, B.A. Peptaibols: Models for ion channels. *Biochem. Soc. Trans.* **2001**, *29*, 565–570. [CrossRef] [PubMed]
21. Wu, G.; Dentinger, B.T.M.; Nielson, J.R.; Peterson, R.T.; Winter, J.M. Emerimicins V–X, 15-Residue Peptaibols Discovered from an *Acremonium* sp. through Integrated Genomic and Chemical Approaches. *J. Nat. Prod.* **2021**, *84*, 1113–1126. [CrossRef] [PubMed]
22. Siebert, A.; Wysocka, M.; Krawczyk, B.; Cholewiński, G.; Rachoń, J. Synthesis and Antimicrobial Activity of Amino Acid and Peptide Derivatives of Mycophenolic Acid. *Eur. J. Med. Chem.* **2018**, *143*, 646–655. [CrossRef] [PubMed]

Disclaimer/Publisher's Note: The statements, opinions and data contained in all publications are solely those of the individual author(s) and contributor(s) and not of MDPI and/or the editor(s). MDPI and/or the editor(s) disclaim responsibility for any injury to people or property resulting from any ideas, methods, instructions or products referred to in the content.